Electromagnetic Power Deposition in a Dielectric Cylinder in the Presence of a Reflecting Surface

R. RUPPIN

Abstract—**A method for calculating electromagnetic power absorption in a dielectric cylinder in the presence of a reflecting plane, due to irradiation by a normally incident plane wave, is presented. The method, which combines imaging with point matching, is applied to the calculation of the absorbed power density in tissue cylinders of arm and thigh size.**

I. Introduction

DETAILED theoretical investigations of the interaction of electromagnetic waves with biological bodies have been performed in recent years. The wide range of geometries considered by various researchers included slabs [1], [2], spheres [3]–[10], cylinders [11], [12], spheroids [13]–[17], ellipsoids [18], [19], and shapes approximating human torsos [20]. In calculations of this type it was usually assumed that the interaction between the electromagnetic wave and the biological body takes place in free space. However, in the evaluation of potential hazards it is important to incorporate the effects of the surroundings because these may cause substantial increases in the absorption rate. Bernardi *et al.* [21] have calculated the power absorbed in a layered slab of infinite extent in the presence of a perfectly reflecting screen. This, however, is an oversimplified model from which it is difficult to draw conclusions about the absorption rate in biological bodies of finite extent. One of the main drawbacks of the slab model is that when the slab is thick enough (in practice, thicker than 40 cm) the presence of the screen is irrelevant. Gandhi *et al.* [22] have recently performed absorption measurements on scaled figurines and on rats in the presence of flat reflectors. In the absence of an exact theory for the effects of reflectors on the absorption rate, they employed antenna theory formulas instead. In this paper we present a new method, which combines imaging with point matching, to obtain the absorption rate in a dielectric cylinder near a perfectly reflecting plane. The method is applied to tissue cylinders of radii corresponding to arm and thigh sizes.

II. Theory

The geometry which we consider is shown in Fig. 1. An infinite circular cylinder of radius R is located at a distance d from an infinite perfectly conducting plane. The cylinder material is characterized by a complex dielectric constant ϵ. A plane wave is incident normally, and our aim is to calculate the energy absorption rate in the cylinder. We discuss the two independent polarizations separately.

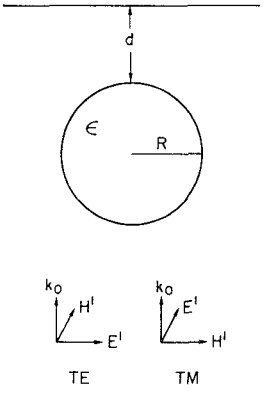

Fig. 1. Geometry of dielectric cylinder located at a distance d from a perfectly conducting plane, with normally incident TE or TM wave.

A. TE Polarization

The incident fields are given by

$$\boldsymbol{E}^i = E_0 \exp(ik_0 x)\boldsymbol{a}_y \tag{1a}$$

$$\boldsymbol{H}^i = \frac{k_0}{\omega\mu_0} \exp(ik_0 x)\boldsymbol{a}_z \tag{1b}$$

where $k_0 = \omega(\mu_0\epsilon_0)^{1/2}$ and $\boldsymbol{a}_y$ and $\boldsymbol{a}_z$ are unit vectors along the y and z axes, respectively. In the absence of the cylinder the wave reflected from the conducting plane would have the form

$$\boldsymbol{E}^r = -E_0 \exp\left[2ik_0(R+d)\right] \exp(-ik_0 x)\boldsymbol{a}_y \tag{2a}$$

$$\boldsymbol{H}^r = \frac{k_0}{\omega\mu_0} E_0 \exp\left[2ik_0(R+d)\right] \exp(-ik_0 x)\boldsymbol{a}_z. \tag{2b}$$

In order to satisfy all the boundary conditions we add to the fields in the air, given by (1) and (2), two scattered waves, which we expand in terms of the following cylindrical vector wave functions [23]:

$$\boldsymbol{M}_n^0(\boldsymbol{r}) = \frac{1}{k_0} \nabla \times \left[\boldsymbol{a}_z H_n(k_0 r) e^{in\phi}\right] \tag{3a}$$

Manuscript received January 2, 1979; revised June 15, 1979.
The author is with the Israel Atomic Energy Commission, Soreq Nuclear Research Centre, Yavne 70600, Israel.

0018-9480/79/1100-0910$00.75 ©1979 IEEE

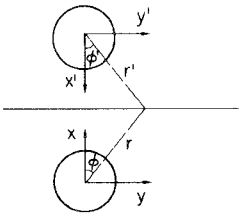

Fig. 2. The cylinder and its image and the two corresponding coordinate systems.

$$N_n^0(r)=\frac{1}{k_0}\nabla\times M_n^0(r) \tag{3b}$$

where H_n is the cylindrical Hankel function. The fields scattered from the dielectric cylinder are written in the form

$$E^{s1}=iE_0\sum_{n=-\infty}^{\infty} i^n a_n^1 M_n^0(r) \tag{4a}$$

$$H^{s1}=\frac{k_0}{\omega\mu_0}E_0\sum_{n=-\infty}^{\infty} i^n a_n^1 N_n^0(r). \tag{4b}$$

Another scattered wave originates from the image cylinder shown in Fig. 2. This wave is expanded in the form

$$E^{s2}=iE_0\sum_{n=-\infty}^{\infty} i^n a_n^2 M_n^0(r') \tag{5a}$$

$$H^{s2}=\frac{k_0}{\omega\mu_0}E_0\sum_{n=-\infty}^{\infty} i^n a_n^2 N_n^0(r') \tag{5b}$$

where $r'=(r',\phi',z')$ refers to the origin of a coordinate system centered in the image cylinder (Fig. 2).

The transmitted wave inside the cylinder is written in the form

$$E^t=iE_0\sum_{n=-\infty}^{\infty} i^n b_n M_n^i(r) \tag{6a}$$

$$H^t=\frac{k_i}{\omega\mu_0}E_0\sum_{n=-\infty}^{\infty} i^n b_n N_n^i(r) \tag{6b}$$

where M_n^i and N_n^i are the appropriate vector wave functions inside the cylinder, defined by

$$M_n^i(r)=\frac{1}{k_i}\nabla\times\left[a_z J_n(k_i r)e^{in\phi}\right] \tag{7a}$$

$$N_n^i(r)=\frac{1}{k_i}\nabla\times M_n^i(r) \tag{7b}$$

where J_n is the cylindrical Bessel function and $k_i=\omega(\mu_0\epsilon)^{1/2}$.

Having defined the fields we now impose the boundary conditions. At the conducting plane $x=R+d$ we have the condition

$$E_y^t+E_y^r+E_y^{s1}+E_y^{s2}=0. \tag{8}$$

Since $E_y^i+E_y^r=0$ at $x=R+d$, we have to satisfy the condition $E_y^{s1}+E_y^{s2}=0$ on the plane. From (4a) and (5a) we find that this yields the relation $a_n^2=-a_n^1$, for all n. On the surface of the cylinder $r=R$, the boundary conditions are

$$E_\phi^t+E_\phi^r+E_\phi^{s1}+E_\phi^{s2}=E_\phi^t \tag{9a}$$

$$H_z^i+H_z^r+H_z^{s1}+H_z^{s2}=H_z^t. \tag{9b}$$

Using the expressions (1),(2),(4)–(6), we can write (9) in the form

$$\sum_{n=-\infty}^{\infty}\left(A_n^e a_n^1+B_n^e b_n\right)=f \tag{10a}$$

$$\sum_{n=-\infty}^{\infty}\left(A_n^h a_n^1+B_n^h b_n\right)=g \tag{10b}$$

where

$$A_n^e=i^{n+1}\left\{H_n'(k_0R)e^{in\phi}+\left[\frac{in}{k_0r'}H_n(k_0r')\sin(\phi+\phi')-H_n'(k_0r')\cos(\phi+\phi')\right]e^{in\phi'}\right\} \tag{11}$$

$$B_n^e=-i^{n+1}J_n'(k_iR)e^{in\phi} \tag{12}$$

$$f=\left[\exp(ik_0x)-\exp\left[2ik_0(R+d)\right]\exp(-ik_0x)\right]\cos\phi \tag{13}$$

$$A_n^h=-i^n\left[H_n(k_0R)e^{in\phi}+H_n(k_0r')e^{in\phi'}\right] \tag{14}$$

$$B_n^h=\epsilon^{1/2}i^nJ_n(k_iR)e^{in\phi} \tag{15}$$

$$g=\exp(ik_0x)+\exp(-ik_0x)\exp\left[2ik_0(R+d)\right]. \tag{16}$$

Here ϕ, ϕ', r', and x are the coordinates of any point on the surface $r=R$ of the cylinder. A choice of ϕ determines the corresponding values of ϕ', r', and x. In order to solve the system of equations (10) for the coefficients a_n^1 and b_n, we employ the point-matching method [24]. The symmetry of the problem is such that $a_n^1=a_{-n}^1$ and $b_n=b_{-n}$, for all n. Therefore, if we truncate the expansions (4)–(6) at $n=N$, we will have $2N+2$ unknown coefficients a_0^1, b_0, a_1^1, $b_1,\cdots,a_N^1$, b_N. Imposing the boundary conditions (10) at $N+1$ different points on the surface of the cylinder we obtain $2N+2$ equations and we can solve for the expansion coefficients a_n^1, b_n. From these we then calculate the rate of energy absorption per unit length of the cylinder from

$$W=\frac{1}{2}\int_0^R\int_0^{2\pi}\sigma E^t\cdot E^{t*}d\phi dr=\pi\sigma|E_0|^2\left\{|b_0|^2\int_0^R|J_1(k_ir)|^2rdr+2\sum_{n=1}^{N}|b_n|^2\int_0^R\left[\frac{n^2}{|k_ir|^2}|J_n(k_ir)|^2+|J_n'(k_ir)|^2\right]rdr\right\}. \tag{17}$$

Here σ is the tissue conductivity, which is related to the imaginary part ϵ'' of the dielectric constant ϵ by $\epsilon''=\sigma/\omega\epsilon_0$. The integrations in (17) are performed numerically.

B. TM Polarization

The incident field is given by

$$E^t=E_0\exp(ik_0x)a_z \tag{18a}$$

$$\boldsymbol{H}^i = -\frac{k_0}{\omega\mu_0} E_0 \exp(ik_0 x)\boldsymbol{a}_y. \tag{18b}$$

The reflected wave in the absence of the cylinder is

$$\boldsymbol{E}^r = -E_0 \exp\left[2ik_0(R+d)\right] \exp(-ik_0 x)\boldsymbol{a}_z \tag{19a}$$

$$\boldsymbol{H}^r = -\frac{k_0}{\omega\mu_0} E_0 \exp\left[2ik_0(R+d)\right] \exp(-ik_0 x)\boldsymbol{a}_y. \tag{19b}$$

Again we use two scattered waves. The fields scattered from the cylinder are

$$\boldsymbol{E}^{s1} = iE_0 \sum_{n=-\infty}^{\infty} i^n a_n^1 \boldsymbol{N}_n^0(\boldsymbol{r}) \tag{20a}$$

$$\boldsymbol{H}^{s1} = \frac{k_0}{\omega\mu_0} E_0 \sum_{n=-\infty}^{\infty} i^n a_n^1 \boldsymbol{M}_n^0(\boldsymbol{r}) \tag{20b}$$

and those originating from the image cylinder are

$$\boldsymbol{E}^{s2} = iE_0 \sum_{n=-\infty}^{\infty} i^n a_n^2 \boldsymbol{N}_n^0(\boldsymbol{r}') \tag{21a}$$

$$\boldsymbol{H}^{s2} = \frac{k_0}{\omega\mu_0} E_0 \sum_{n=-\infty}^{\infty} i^n a_n^2 \boldsymbol{M}_n^0(\boldsymbol{r}'). \tag{21b}$$

The fields inside the cylinder are

$$\boldsymbol{E}^t = iE_0 \sum_{n=-\infty}^{\infty} i^n b_n \boldsymbol{N}_n^i(\boldsymbol{r}) \tag{22a}$$

$$\boldsymbol{H}^t = \frac{k_0}{\omega\mu_0} E_0 \sum_{n=-\infty}^{\infty} i^n b_n \boldsymbol{M}_n^i(\boldsymbol{r}). \tag{22b}$$

The boundary condition at the conducting plane

$$E_z^i + E_z^r + E_z^{s1} + E_z^{s2} = 0 \tag{23}$$

holds if $a_n^2 = a_n^1$, for all n. The boundary conditions on the surface of the cylinder $r = R$ are

$$H_\phi^i + H_\phi^r + H_\phi^{s1} + H_\phi^{s2} = H_\phi^t \tag{24a}$$

$$E_z^i + E_z^r + E_z^{s1} + E_z^{s2} = E_z^t \tag{24b}$$

which can again be written in the form (10), but with the following redefinition of the coefficients:

$$A_n^e = i^{n+1}\left[H_n(k_0 R)e^{in\phi} - H_n(k_0 r')e^{in\phi'}\right] \tag{25}$$

$$B_n^e = -i^{n+1} J_n(k_i R)e^{in\phi} \tag{26}$$

$$f = \exp\left[2ik_0(R+d)\right]\exp(-ik_0 x) - \exp(ik_0 x) \tag{27}$$

$$A_n^h = i^n \left\{ -H_n'(k_0 R)e^{in\phi} + \left[\frac{in}{k_0 r'} H_n(k_0 r')\sin(\phi+\phi') - H_n'(k_0 r')\cos(\phi+\phi')\right] e^{in\phi'} \right\} \tag{28}$$

$$B_n^h = \epsilon^{1/2} i^n J_n'(k_i R)e^{in\phi} \tag{29}$$

$$g = \left[\exp(ik_0 x) + \exp|2ik_0(R+d)|\exp(-ik_0 x)\right]\cos\phi. \tag{30}$$

We again truncate the expansions at $n = N$ and obtain the unknown coefficients $a_0^1, b_0, a_1^1, b_1, \cdots, a_N^1, b_N$ by imposing the boundary conditions at $N+1$ different points on the surface of the cylinder. The rate of energy absorption per unit length is

$$W = \pi\sigma|E_0|^2 \left\{ |b_0|^2 \int_0^R |J_0(k_i r)|^2 r dr + 2\sum_{n=1}^{N} |b_n|^2 \int_0^R |J_n(k_i r)|^2 r dr \right\}. \tag{31}$$

III. Numerical Results and Discussion

We have applied the method developed in Section II to the calculation of the absorption in tissue cylinders of two sizes, $R = 5$ cm (arm size) and $R = 10$ cm (thigh size). The dielectric constant of the cylinder material was taken from the data given by Johnson and Guy [25] for tissues with high water content. The value of N at which the summations (4)–(6), (10), and (20)–(22) were truncated was chosen large enough, so that no significant change in the calculated absorption was noticed upon increasing it to $N+1$. N and the corresponding size of the system of equations tend to increase with R and also with ω. For the examples discussed here, the value $N = 4$ was found to be satisfactory over the frequency range of up to 10^3 MHz. In Figs. 3–6 the frequency dependence of the specific absorption rate (SAR) is shown for two different distances from the metallic wall. The SAR was obtained from W by dividing by πR^2. Also shown, for comparison, is the SAR in the same cylinders in free space, i.e., without the metallic reflector. This was calculated from standard scattering theory formulas [24]. When comparing with the absorption in the free-space case, we find that in the TE case (Figs. 3 and 4) and $d = 0$ (the cylinder touching the wall) there occurs a large enhancement over the whole frequency range considered. For a distance of 50 cm from the wall the behavior is similar at the lowest frequencies, but there appear oscillations for frequencies higher than about 100 MHz. In the TM case (Figs. 5 and 6) and $d = 0$ the absorption at the lower frequencies is reduced considerably, but it rises and becomes slightly higher than the free-space absorption for frequencies higher than about 100 MHz. For a distance of 50 cm the transition from the region of reduced absorption to that of enhanced absorption occurs at a lower frequency of about 30 MHz. The oscillatory character of the calculated SAR, which becomes more prominent as d increases, reflects the interference between the fields incident directly on the cylinder, (1a) and (1b), and the fields which are reflected from the conducting plane, (2a) and (2b).

We have presented results for the average SAR only, and not for the absorption pattern inside the cylinder, because the homogeneous cylinder model is too crude for this purpose. However, the method of the present work can also be applied to the more realistic triple layered cylinder model with fat, muscle, and bone layers [11]. We plan to calculate the absorption pattern in such a cylinder

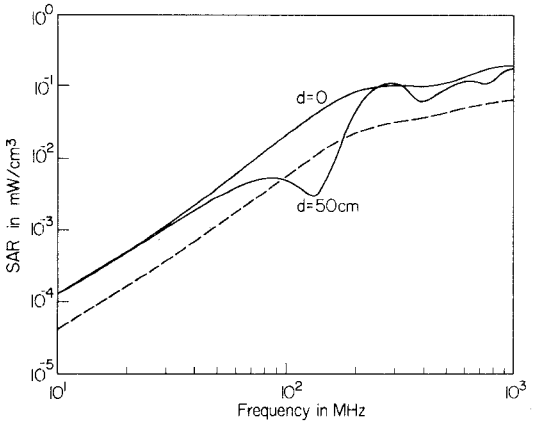

Fig. 3. Average SAR in a tissue cylinder of radius 5 cm at distance d from a reflecting wall. The incident wave is TE polarized and has a power density of 1 mW/cm^2. The dashed curve shows the result for the free-space case.

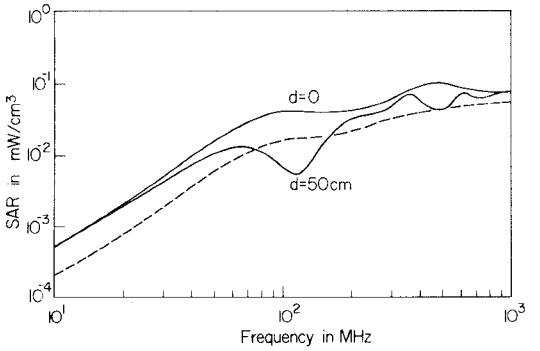

Fig. 4. Average SAR in a tissue cylinder of radius 10 cm at distance d from a reflecting wall. The incident wave is TE polarized and has a power density of 1 mW/cm^2. The dashed curve shows the result for the free-space case.

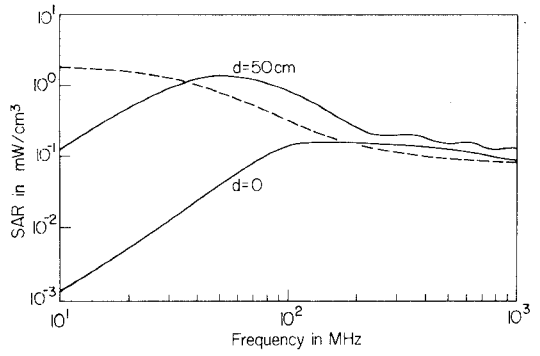

Fig. 5. Average SAR in a tissue cylinder of radius 5 cm at distance d from a reflecting wall. The incident wave is TM polarized and has a power density of 1 mW/cm^2. The dashed curve shows the result for the free-space case.

near a conducting wall in the future. Furthermore, as the infinite cylinder is an oversimplified model of an arm or a thigh at lower frequencies [26], we suggest that dielectric bodies of finite extent (e.g., spheres, spheroids, or finite cylinders) near reflecting surfaces can also be treated by the above presented method of imaging combined with point matching.

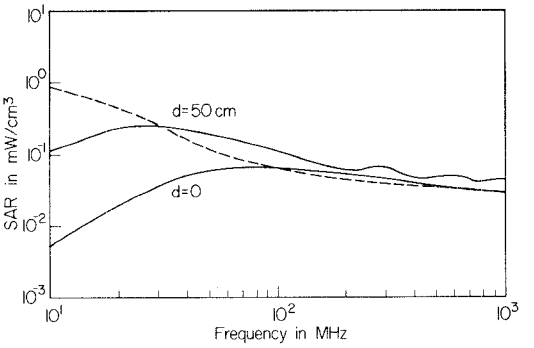

Fig. 6. Average SAR in a tissue cylinder of radius 10 cm at distance d from a reflecting wall. The incident wave is TM polarized and has a power density of 1 mW/cm^2. The dashed curve shows the result for the free-space case.

References

[1] H. P. Schwan and K. Li, "Hazards due to total body irradiation by radar," *Proc IRE*, vol. 44, pp. 1572–1581, Nov. 1956.

[2] C. C. Johnson, C. H. Durney, and H. Massoudi, "Electromagnetic power absorption in anisotropic tissue media," *IEEE Trans. Microwave Theory Tech.*, vol. MTT-23, pp. 529–532, June 1975.

[3] A. R. Shapiro, R. F. Lutomirski, and H. T. Yura, "Induced fields and heating within a cranial structure irradiated by an electromagnetic plane wave," *IEEE Trans. Microwave Theory Tech.*, vol. MTT-19, pp. 187–196, Feb. 1971.

[4] H. N. Kritikos and H. P. Schwan, "Hot spots generated in conducting spheres by electromagnetic waves and biological implications," *IEEE Trans. Biomed. Eng.*, vol. BME-19, pp. 53–58, Jan. 1972.

[5] J. C. Lin, A. W. Guy, and C. C. Johnson, "Power deposition in a spherical model of man exposed to 1–20 MHz electromagnetic fields," *IEEE Trans. Microwave Theory Tech.*, vol. MTT-21, pp. 791–797, Dec. 1973.

[6] H. S. Ho, "Contrast of dose distribution in phantom heads due to aperture and plane wave sources," *Ann. N. Y. Acad. Sci.*, vol. 247, pp. 454–472, Feb. 1975.

[7] H. S. Ho and A. W. Guy, "Calculations of absorbed dose distributions in two sizes of muscle equivalent spheres," *Health Phys.*, vol. 29, pp. 317–324, Aug. 1975.

[8] H. N. Kritikos and H. P. Schwan, "The distribution of heating potential inside lossy spheres," *IEEE Trans. Biomed. Eng.*, vol. BME-22, pp. 457–463, Nov. 1975.

[9] C. M. Weil, "Absorption characteristics of multilayered sphere models exposed to UHF/microwave radiation," *IEEE Trans. Biomed. Eng.*, vol. BME-22, pp. 468–476, Nov. 1975.

[10] H. N. Kritikos and H. P. Schwan, "Formation of hot spots in multilayered spheres," *IEEE Trans. Biomed. Eng.*, vol. BME-23, pp. 168–172, Mar. 1976.

[11] H. S. Ho, "Energy absorption patterns in circular triple-layered tissue cylinders to plane wave sources," *Health Phys.*, vol. 31, pp. 97–108, Aug. 1976.

[12] T. K. Wu and L. L. Tsai, "Electromagnetic fields induced inside arbitrary cylinders of biological tissue," *IEEE Trans. Microwave Theory Tech.*, vol. MTT-25, pp. 61–65, Jan. 1977.

[13] C. H. Durney, C. C. Johnson, and H. Massoudi, "Long wavelength analysis of plane wave irradiation of a prolate spheroid model of man," *IEEE Trans. Microwave Theory Tech.*, vol. MTT-23, pp. 246–253, Feb. 1975.

[14] C. C. Johnson, C. H. Durney, and H. Massoudi, "Long wavelength electromagnetic power absorption in prolate spheroidal models of man and animals," *IEEE Trans. Microwave Theory Tech.*, vol. MTT-23, pp. 739–747, Sept. 1975.

[15] P. W. Barber, "Electromagnetic power deposition in prolate spheroid models of man and animals at resonance," *IEEE Trans. Biomed. Eng.*, vol. BME-24, pp. 513–521, Nov. 1977.

[16] ——, "Scattering and absorption efficiencies for nonspherical dielectric objects—biological models," *IEEE Trans. Biomed. Eng.*, vol. BME-25, pp. 155–159, Mar. 1978.

[17] R. Ruppin, "Calculation of electromagnetic energy absorption in

prolate spheroids by the point matching method," *IEEE Trans. Microwave Theory Tech.*, vol. MTT-26, pp. 87–90, Feb. 1978.
[18] H. Massoudi, C. H. Durney, and C. C. Johnson, "Long wavelength analysis of plane wave irradiation of an ellipsoidal model of man." *IEEE Trans. Microwave Theory Tech.*, vol. MTT-25, pp. 41–46, Jan. 1977.
[19] ——, "Long wavelength electromagnetic power absorption in ellipsoidal models of man and animals," *IEEE Trans. Microwave Theory Tech.*, vol. MTT-25, pp. 47–52, Jan. 1977.
[20] K. M. Chen and B. S. Guru, " Internal EM field and absorbed power density in human torsos induced by 1–500 MHz EM waves," *IEEE Trans. Microwave Theory Tech.*, vol. MTT-25, pp. 746–756, Sept. 1977.
[21] P. Bernardi, F. Giannini, and R. Sorrentino, "Effects of the surroundings on electromagnetic power absorption in layered tissue media," *IEEE Trans. Microwave Theory Tech.*, vol. MTT-24, pp. 621–625, Sept. 1976.
[22] O. P. Gandhi, E. L. Hunt, and J. A. D'Andrea, "Deposition of electromagnetic energy in animals and in models of man with and without grounding and reflector effects," *Radio Sci.*, vol. 12, Suppl., pp. 39–47, Dec. 1977.
[23] J. A. Stratton, *Electromagnetic Theory*. New York: McGraw-Hill, 1941.
[24] M. Kerker, *The Scattering of Light and Other Electromagnetic Radiation*. New York: Academic, 1969.
[25] C. C. Johnson and A. W. Guy, "Nonionizing electromagnetic wave effects in biological materials and systems," *Proc. IEEE*, vol. 60, pp. 692–718, June 1972.
[26] H. Massoudi, C. H. Durney, and C. C. Johnson, "The geometrical optics solution and the exact solution for internal fields and SAR in a cylindrical model of man irradiated by an electromagnetic plane wave," *Radio Sci.*, to be published.

A Possible Mechanism for the Influence of Electromagnetic Radiation on Neuroelectric Potentials

RONALD J. MACGREGOR

***Abstract*—This paper explores the idea that the electrical component of applied microwave and radiowave radiation might induce transmembrane potentials in nerve cells and, thereby, disturb nervous function and behavior. The paper estimates the transmembrane currents and potentials induced in nerve cells by applied electrical fields and currents. Estimates are made for steady and for oscillating stimulation. The primary conclusion is that intracranial electrical fields associated with low-intensity irradiation in the frequency range of 10^6–10^{10} Hz may induce transmembrane potentials of tenths of millivolts (or more) and that, therefore, such externally applied fields may distrub normal nervous function through this mechanism. The paper also presents a discussion which indicates that the induced transmembrane potential should exhibit a maximum at about 10^8 Hz. Although some researchers suggest that the direct mechanism explored here may not represent the main influence of microwaves and radiowaves on biological tissue, this model together with a recent model by Barnes and Hu [21] suggest that the results so produced may indeed be significant.**

I. INTRODUCTION

THERE IS a wide collection of intriguing phenomena concerning the influence of applied fields and currents on nervous function and behavior. Steady electric fields and currents applied to the brain are known to induce a variety of behavioral responses, ranging from hallucinations or the vivid reexperiencing of past events to the performance of coordinated complex motor patterns or the exhibition of rage or fright [1]. Stimulating steady currents are used extensively to activate nerve cells in neurophysiological research [2]. Such experiments are used to investigate basic neuroelectric mechanisms and to examine interconnecting pathways among cells. Less well known in this country is a large body of research carried out in the Soviet Union which indicates that low-intensity electromagnetic radiation may induce insomnia, irritability, loss of memory, fatigue, headache, tremor, hallucinations, automatic disorders, or disturbed sensory sensitivity in humans [3]. These effects seem to occur primarily in the microwave and radiowave region and at mean intensities well below safety standards currently in use for long-term exposure. In this country, Frey has shown that both low-intensity microwave and radiowave radiation applied to the head induces auditory perception in human subjects and neuroelectric potential fluctuations in the brain stem of cats [4]. Reviews of the influence of microwaves and radiowaves on neural function are contained in [3], [5],

Manuscript received April 14, 1977; revised May 17, 1978. An earlier version of this model has been preprinted by the Rand Corporation, Santa Monica, CA, as P-4398, June 1970.

The author is with the Department of Electrical Engineering, University of Colorado, Boulder, CO 80309.

0018-9480/79/1100-0914$00.75 ©1979 IEEE